Joint characterization of vegetation by satellite observations from visible to microwave wavelengths: A sensitivity analysis

Catherine Prigent [1] and Filipe Aires

Department of Applied Physics, Columbia University, NASA Goddard Institute for Space Studies
New York, New York

William Rossow and Elaine Matthews

NASA Goddard Institute for Space Studies, New York, New York

Abstract. This study presents an evaluation and comparison of visible, near-infrared, passive and active microwave observations for vegetation characterization, on a global basis, for a year, with spatial resolution compatible with climatological studies. Visible and near-infrared observations along with the Normalized Difference Vegetation Index come from the Advanced Very High Resolution Radiometer. An atlas of monthly mean microwave land surface emissivities from 19 to 85 GHz has been calculated from the Special Sensor Microwave / Imager for a year, suppressing the atmospheric problems encountered with the use of simple channel combinations. The active microwave measurements are provided by the ERS-1 scatterometer at 5.25 GHz. The capacity to discriminate between vegetation types and to detect the vegetation phenology is assessed in the context of a vegetation classification obtained from in situ observations. A clustering technique derived from the Kohonen topological maps is used to merge the three data sets and interpret their relative variations. NDVI varies with vegetation density but is not very sensitive in semi-arid environments and in forested areas. Spurious seasonal cycles and large spatial variability in several areas suggest that atmospheric contamination and/or solar zenith angle drift still affect the NDVI. Passive and active microwave observations are sensitive to overall vegetation structure: they respond to absorption, emission, and scattering by vegetation elements, including woody parts. Backscattering coefficients from ERS-1 are not sensitive to atmospheric variations and exhibit good potential for vegetation discrimination with ~10 dB dynamic range between rain forest to arid grassland. Passive microwave measurements also show some ability to characterize vegetation but are less sensitive than active measurements. However, passive observations show sensitivity to the underlying surface wetness that enables detection of wetlands even in densely vegetated areas. Merging the data sets using clustering techniques capitalizes on the complementary strengths of the instruments for vegetation discrimination and shows promising potential for land cover characterization on a global basis.

1. Introduction

Physical characteristics of land cover are one family of crucial boundary conditions for climate models because they can strongly influence the exchanges of energy, water, and carbon between the biosphere and the at-

mosphere. Land surface parameterizations for General Circulation Models have traditionally relied on global fields of terrestrial biophysical parameters estimated from land cover data sets derived from in situ surveys [*Matthews*, 1983] or from vegetation indices calculated from satellite data in the visible and near-infrared [*Sellers et al.*, 1994, 1996]. The Normalized Difference Vegetation Index (NDVI), calculated from the red and near-infrared channels of the Advanced Very High Resolution Radiometer (AVHRR), has been extensively used for vegetation studies. The availability of the NDVI data for two decades and its high horizontal spatial resolution (up to 1 km) have motivated a large number of studies

[1]Now at Département de Radioastronomie Millimétrique /CNRS, Observatoire de Paris, Paris.

from regional to global scales [e.g., *Tucker et al.*, 1985; *Myneni et al.*, 1998; *DeFries et al.*, 1999], relating NDVI to vegetation physiology and structure. However, there are growing concerns about the ability of the NDVI to quantitatively represent the vegetation properties, and NDVI sensitivity to atmospheric contamination and instrument calibration is debated [*Gutman*, 1999].

Lower-resolution space-borne sensors operating in the microwave part of the spectrum have also shown some ability to characterize the land surface at spatial resolutions compatible with climatological applications. For global vegetation characterization, these instruments have, to date, triggered less interest than their visible and near-infrared counterparts.

Passive microwave observations from the Scanning Multichannel Microwave Radiometer on board Nimbus 7 starting in 1978 and from the Special Sensor Microwave/ Imager (SSM/I) on board Defense Meteorological Satellite Program (DMSP) satellites since 1987 have been used in vegetation studies, especially in conjunction with NDVI responses. Most studies have focused on the use of simple indices like the microwave vegetation index which is based on the polarization difference at 37 GHz [e.g., *Choudhury and Tucker*, 1987; *Justice et al.*, 1989]. However, as noted by several authors [*Tucker*, 1989; *Kerr and Njoku*, 1993], atmospheric effects, especially cloud cover, is responsible for a large part of the 37 GHz polarization difference, casting doubt on the interpretation of simple indices solely in terms of surface properties. Recently, *Prigent et al.* [1997, 1998] calculated land surface microwave emissivities from SSM/I observations by removing contributions from the atmosphere, clouds, and rain using ancillary satellite data. These global results show promising correspondences between geographical and seasonal patterns of emissivities and land surface characteristics.

Multiyear active microwave data over the entire globe are a relatively new resource available since July 1991 with the launch of the European Remote Sensing (ERS) satellite ERS-1 carrying a wind scatterometer operating at 5.25 GHz (C band). Scatterometers provide measurements of the backscattering coefficient of observed surfaces. Although primarily designed for estimating wind speed and direction over the ocean, space-borne scatterometers have shown good correlation with vegetation dynamics at global and regional scales. Preliminary results were obtained using 3 months of scatterometer data obtained from Seasat-A in 1978 [*Kennett and Li*, 1989] and were later confirmed by several authors using ERS-1 and ERS-2 data [*Kerr and Magnani*, 1993; *Wismann et al.*, 1993; *Frison and Mougin*, 1996a, b; *Wagner et al.*, 1999a]. Other studies [e.g., *Wagner et al.*, 1999b] have also shown that the backscattering coefficients measured by ERS-1 are sensitive to soil moisture.

The objective of this study is to compare individually and together the ability of these measurements to characterize the spatial distribution of the vegetation and its phenology and to examine how complementary strengths of these instruments can be used to obtain maximum information about vegetation physical characteristics on a global basis. The three types of observations analyzed here cover a large portion of the electromagnetic spectrum: (1) AVHRR visible (0.58-0.68 μm) and near-infrared (0.73-1.1 μm) reflectances and the derived NDVI, (2) passive microwave SSM/I emissivities between 19 and 85 GHz (i.e., from 1.58 to 0.35 cm in wavelength), and (3) ERS-1 active instrument backscattering coefficient at 5.25 GHz (wavelength = 5.71 cm). Our analysis of SSM/I also uses observations in the visible and infrared ($\sim$ 11 μm) to identify cloud-free scenes and measure surface skin temperatures. However, in this study we do not consider the possible information about land-surface properties that may be obtained from temperature data.

A year of monthly mean or monthly composite observations of each instrument is examined, at a spatial resolution of 0.25° × 0.25° at the equator. This spatial resolution was chosen to be appropriate for global climate studies. The three data sets are described in section 2. Section 3 briefly reviews the responses of each wavelength range to the land surface characteristics, as background in interpreting the monthly distribution of the data sets. The ability of each instrument to discriminate among vegetation types and to capture the seasonal cycle is analyzed on a global basis (section 4). The vegetation classification [*Matthews*, 1983] is used as a reference. A clustering technique derived from *Kohonen* [1984] topological maps is implemented to merge the three data sets and enable a synthetic analysis of the respective variations of the spectral bands (section 5). Section 6 concludes this study and suggests potential applications of the clustering technique for land cover classification.

2. Data Sets

This study evaluates the potential of globally and routinely available satellite data for their potential for vegetation characterization with a spatial resolution compatible with climatological studies. A full annual cycle of the data sets from three satellites (July 1992 to June 1993) is analyzed. All the data sets are mapped on an equal-area grid of 0.25°×0.25° resolution at the equator and monthly mean or monthly composite values are calculated from daily values.

High-resolution data from visible and near-infrared (e.g., Landsat and Spot) or from synthetic aperture radar (SAR) have been used for local studies. However, because of large data volumes associated with these observations as well as their incomplete coverage on a global and continuous basis, lower resolution instruments are preferred for global studies.

The three satellite data sets are described in this section along with the *Matthews* [1983] vegetation classification. The latter has been widely used and provides a reference for testing the ability of remote sensing instruments to distinguish among vegetation types.

2.1. Visible and Near-Infrared Reflectances and NDVI From AVHRR

The AVHRR instruments on board the National Oceanic and Atmospheric Administration (NOAA) meteo-

rological polar orbiters provide daily observations of the Earth with a spatial resolution as high as 1 km. The first AVHRR channel is in the visible (VIS 0.58-0.68 μm) where chlorophyll causes absorption of incoming radiation, and the second channel is in the near-infrared (NIR 0.73-1.1 μm). NDVI is calculated as the ratio of the difference of the AVHRR channels 2 and 1 over their sum.

Several AVHRR global data sets have been produced. Monthly composite AVHRR products at 8 km resolution are generated under the joint NASA and NOAA Earth Observing System Pathfinder project [*James and Kalluri*, 1994]. They are available at NASA Goddard Space Flight Center Distributed Active Archived Center (Web site http://gsfc.nasa.gov), along with a description of the data calibration and processing. Corrections for Rayleigh scattering and ozone absorption are performed, but there is no atmospheric correction for water vapor and aerosols. However, NDVI composite maps correspond to the maximum value of the NDVI for the compositing time period, which tends to minimize atmospheric contamination [*Holben*, 1986]. A cloud screening procedure is performed. Solar zenith angle dependences are related to both annual solar cycle and changes in equatorial crossing time. They are not accounted for in the reflectances and can introduce a spurious seasonal variation in the NDVI signal that may be falsely attributed to vegetation changes [*Gutman*, 1999]. *Gutman* [1999] describes the data set in detail and analyzes its quality. He reviews instrument performance and satellite orbit characteristics. For NOAA 11, which covers the period of this study, anomalies in channel 1 and 2 reflectances should be no more than $\pm 1\%$ and $\pm 2\%$, respectively [*Gutman*, 1999]. Using a simple error propagation equation, these errors translate into an accuracy of ~ 0.1 in the NDVI for typical values of the VIS and NIR reflectances. Several problems are mentioned (intersensor calibration, sensor degradation, satellite drift and changes in the solar zenith angle, contamination by clouds, water vapor, aerosols, and ozone) that hamper the interpretation of NDVI as a purely land surface signal. From radiative transfer calculations, *Tanré et al.* [1992] carefully quantify the effect of atmospheric constituents on VIS and NIR reflectances. Water vapor absorption essentially affects NIR reflectances, depressing it by 10-30% in sparsely vegetated areas. That translates into a decrease of up to 0.1 in the NDVI. Ozone can reduce the reflectance in channel 1 by 5-15% of its value. Aerosols can completely mask vegetation properties with NDVI changes up to 0.2 in densely vegetated areas. *Gutman* [1999] draws attention to these NDVI problems stressing that NDVI investigations, especially those directed at long-term trends, currently encounter serious challenges.

VIS and NIR reflectances and the NDVI monthly composite products are investigated in this study. Data are averaged from their 8 km Pathfinder nominal resolution to an equal-area grid of 0.25° × 0.25° at the equator.

2.2. Microwave Emissivities Between 19 and 85 GHz (SSM/I)

The SSM/I instruments on board the DMSP polar orbiters observe the Earth twice daily at 19.35, 22.235, 37.0, and 85.5 GHz with both vertical and horizontal polarizations, with the exception of 22 GHz which is vertical polarization only [*Hollinger et al.*, 1987]. The observing incident angle is close to 53°, and the elliptical fields of view decrease in size proportionally with frequency, from 43 × 69 to 13 × 15 km². *Hollinger et al.* [1990] provide an evaluation of the instruments, and intersensor calibration was examined by *Colton and Poe* [1999]. Pioneer investigations of the sensitivity of passive microwave to vegetation used linear combinations of channels [e.g., *Choudhury and Tucker*, 1987]. However, these simple indices have been shown to be contaminated by variations in atmospheric parameters and surface temperature. Microwave emissivities of land surfaces were recently estimated from SSM/I observations by removing contributions from the atmosphere, clouds, and rain using ancillary data from the International Satellite Cloud Climatology Project (ISCCP) [*Rossow and Schiffer*, 1991, 1999; *Rossow et al.*, 1996] and the National Centers for Environmental Prediction (NCEP analyses) [*Kalnay et al.*, 1996]. The method is fully described by *Prigent et al.* [1997, 1998] and summarized here. Cloud-free SSM/I observations are first isolated using collocated visible/infrared satellite observations (ISCCP data). The cloud-free atmospheric contribution is then calculated from an estimate of the local atmospheric temperature-humidity profile from NCEP reanalysis. The atmospheric contribution varies spatially and reaches 15% and 50% in the tropics for 19 and 85 GHz, respectively. Finally, with the surface skin temperature derived from IR observations (ISCCP estimate), the surface emissivity is calculated for all seven SSM/I channels. The standard deviation of day-to-day variations of the emissivities retrieved over a month are typically 0.013 for all channels and for their polarization differences which is a measure of the precision of these estimates. Monthly mean values are calculated with a spatial resolution of 0.25° at the equator.

2.3. Microwave Backscattering at 5.25 GHz (ERS-1 Scatterometer)

The European Space Agency (ESA) ERS wind scatterometer operates at 5.25 GHz vertical polarization with a 50 km spatial resolution. General characteristics and performance of the ERS scatterometer are given by *Frison and Mougin* [1996a]. The backscattering signal is continuously measured by three antennas, one looking normal to the satellite flight path and the other two pointing 45° forward and backward, respectively. The instrument scans a 500 km wide swath with viewing angles ranging from 18° to 59°. The ERS scatterometer shares some hardware with the synthetic aperture radar (SAR) and the SAR and the scatterometer modes are mutually exclusive. Therefore, over some areas where the SAR is typically on (North America

and Europe), the temporal sampling rate for the scatterometer is low. With the scatterometer operating continuously, global coverage would be achieved in about 4 days. The scatterometer response is very stable over time for nonchanging targets, and the measurement uncertainty is estimated to be about 5%. Water vapor and cloud absorption/emission are negligible at 5.25 GHz, and no atmospheric correction is required for the scatterometer signal. *Frison and Mougin* [1996a] show that the antenna intercalibration is very good, which enables the use of all three antennas. They also demonstrate that azimuth angle effects are small over vegetated surfaces, although strong anisotropic signatures are observed over some deserts. For incidence angles between 25° and 50°, scatterometer responses can be approximated by a linear function of the incidence angle. *Frison and Mougin* [1996b] compared the scatterometer responses at various incidence angles and showed that the radar signal at low incidence angles ($\leq 20°$) is related to soil characteristics, whereas observations at large incidence angles ($\sim 45°$) provide more information about vegetation. In addition, radar signals at low incidence angles exhibit a larger scatter and a smaller dynamic range over the course of a year. Other studies [e.g., *Wagner et al.*, 1999a] recommend fitting a model to the slope of the angular dependence at 40°, because this parameter is considered to be less sensitive to soil moisture. However, this parameter is very sensitive to noise, and several years of data are required to calculate it. Following the method developed by *Frison and Mougin* [1996a], for each cell on an equal-area grid of 0.25°×0.25° at the equator, a linear fit is calculated for all incidence angles between 25° and 50° for a month and the fitted value at 45° is kept.

2.4. Matthews' Vegetation Classification

Matthews [1983] vegetation and land use data set was compiled from a large number of published sources. At a 1° spatial resolution the vegetation classification distinguishes a large number of vegetation types, typically grouped to 30 classes of natural vegetation. Associ-

Table 1. Matthews' Vegetation Classification [a]

Vegetation Types		Pixel Numbers		
31 classes	10 classes	Northern Hemisphere	Southern Hemisphere	Description
1	1	5942	10,149	tropical evergreen rain forest, mangrove
2	3	3654	621	tropical/subtropical evergreen seasonal broad-leaved forest
3	1	0	231	subtropical evergreen rain forest
4	3	0	479	temperate/subpolar evergreen rain forest
5	3	780	134	temperate evergreen seasonal broad-leaved forest, summer rain
6	5	322	236	evergreen broad-leaved sclerophyllous forest, winter rain
7	3	618	0	tropical/subtropical evergreen needle-leaved forest
8	3	11,921	0	temperate/subpolar evergreen needle-leaved forest
9	2	1823	1647	tropical/subtropical drought-deciduous forest
10	2	5559	95	cold-deciduous forest, with evergreens
11	2	4598	0	cold-deciduous forest, without evergreens
12	8	718	2624	xeromorphic forest/woodland
13	5	695	1408	evergreen broad-leaved sclerophyllous woodland
14	5	3227	0	evergreen needle-leaved woodland
15	4	1767	3438	tropical/subtropical drought-deciduous woodland
16	4	3240	0	cold-deciduous woodland
17	8	1357	272	evergreen broad-leaved shrubland/thicket and dwarf shrubland
18	8	817	41	evergreen needle-leaved or microphyllous shrubland/thicket
19	8	844	214	drought-deciduous shrubland/thicket and dwarf shrubland/thicket
20	8	601	0	cold-deciduous subalpine/subpolar shrubland and dwarf shrubland
21	8	6258	5279	xeromorphic shrubland/dwarf shrubland
22	7	9482	8	arctic/alpine tundra/mossy bog
23	6	3781	4587	tall/medium/short grassland with 10-40% tree cover
24	6	3168	1808	tall/medium/short grassland with <10% tree or tuft-plant cover
25	6	8839	3374	tall/medium/short grassland with shrub cover
26	6	598	438	tall grassland, no woody cover
27	6	560	436	medium grassland, no woody cover
28	6	4872	2724	meadow/short grassland, no woody cover
29	6	359	0	forb formation
30	9	18,187	1934	desert (bare soil)
31	10	24,965	2896	cultivation

[a] The 31 vegetation classes are defined by *Matthews* [1983]. The number of equal area pixels of 0.25° × 0.25° at the equator is indicated for each vegetation type and for each hemisphere. Each pixel surface is 773 km^2. The 10-class vegetation classification is also defined, in relation to the Matthews' original classification.

ated with the vegetation classification is a land use data set that distinguishes five levels of cultivation intensity, ranging from 0 to 100% cultivation for 1° cells. Combining the vegetation and land use data set gives information about actual land cover. Table 1 presents Matthews' vegetation classification for the 30 vegetation classes, along with a simplified nine-class grouping primarily on the basis of life form. For each vegetation class, areas with cultivation intensity of > 20% are defined as cultivation, which makes up a tenth class. Vegetation types in the 10-class grouping are denoted by Vn, and those in the 31-class grouping by vn.

3. Overview of Wavelength Responses to Surface Characteristics and Presentation of Monthly Maps

3.1. Visible and Near-Infrared Reflectances and the NDVI

Green vegetation exhibits a characteristic reflectance curve. Snow-free reflectance is ~ 0.05 in the VIS portion of the spectrum (≤ 0.7 μm) with a steep rise in the NIR (0.7-1.1 μm) to about 0.20. Seasonally, the rise of full-spectrum albedo from the beginning to the peak of the growing season is the net effect of two opposing trends [Bauer and Dutton, 1962; Pinty and Szejwach, 1985]. The spring-summer increase is governed by declining reflectance in the VIS and increasing reflectance in the NIR. Full-spectrum albedo declines from the growing season maximum through a reversal of these VIS and NIR trends. These seasonal variations result in a NIR/VIS ratio that increases during the growing season and declines abruptly at the end of the growing season. The growing season minimum in the VIS is due primarily to chlorophyll absorption at ~ 0.65 μm [Knipling, 1970]. Individual leaves do not absorb NIR radiation significantly, and NIR reflectance of vegetation canopy is due to complex interactions within the internal leaf structure and between the leaves, the canopy structure, and the soil background [Scott et al., 1968; Knipling, 1970; Sinclair et al., 1971; Gausman, 1974]. Colwell [1974] insists on the important role of vegetation structure, soil reflectance, and observation geometry (especially solar zenith angle) in understanding and predicting vegetation canopy from NDVI. From ground-based measurements, several authors have noted the difficulty of differentiating between vegetation types from reflectances only [Scott et al., 1968; Sinclair et al., 1971] and suggest exploring the temporal changes of the reflectances. Tucker [1979] showed correlation between the properties of the vegetation canopy and the reflectances (in the VIS at 0.65 μm and in the NIR), whereas Scott et al. [1968] only observed such a correlation in the VIS.

Different combinations of the reflectances in the VIS at 0.65 μm and the NIR have been investigated [e.g., Tucker, 1979; Begue and Myneni, 1996]. They are all sensitive to the presence of vegetation but are differentially affected by changes in soil color and brightness.

NDVI, the most widely used, capitalizes on the magnitude and seasonal variations of reflectance differences between spectral bands.

NDVI has been found to be correlated with the Fraction of Photosynthetically Active Radiation absorbed by green vegetation (since it is related to spectral albedo), to Leaf Area Index [e.g., Asrar et al., 1984; Begue and Myneni, 1996], and to carbon uptake and release by vegetation [Fung et al., 1987], as well as providing information about vegetation phenology [Moulin et al., 1997].

3.2. Passive and Active Microwave Responses Over Land

Microwave responses to the land surface include contributions from the vegetation and from the underlying surface. An extensive body of research has been directed toward a better understanding of the mechanisms responsible for the microwave emission and backscattering of soil and vegetation, both from theoretical analysis and from small-scale field experiments using hand-held, truck-mounted, or airborne sensors. A review of these studies is presented by Ulaby et al. [1986], and more recent developments include modeling by Karam et al. [1995], Wigneron et al. [1993], Ferrazzoli and Guerriero [1996], and measurements by Matzler [1990], Wigneron et al. [1997], and Hewison [2001].

Vegetation absorbs, emits, and scatters microwave radiation. Radiative properties of vegetation are mainly controlled by the dielectric properties of vegetation components, their density, and the relative size of vegetation components with respect to the wavelength. Dielectric properties of vegetation are closely related to their water content. Increasing vegetation density usually reduces the emissivity polarization difference [Choudhury, 1989] and increases the backscattered signal [Frison and Mougin, 1996a]. Both theory and in situ measurements predict increasing absorption/emission and scattering by vegetation with increasing frequency. As a consequence, the underlying surface contribution is expected to increase with decreasing frequency.

Bare soil response depends on soil dielectric properties and roughness. Smooth bare soils have a quasi-specular reflection, producing high polarization emissivity differences around 50° incidence and low backscattering coefficient. When the terrain gets rougher, surface scattering causes the emissivity polarization difference to decrease and the backscattering coefficient to increase. In dry soil, volume scattering can be involved producing low radar return [Deroin et al., 1997] and specific passive microwave signatures [Prigent et al., 1999].

Water has a high dielectric constant compared to bare soil. For passive measurements, open water surfaces (lakes and inundated areas) exhibit very low emissivities in both horizontal and vertical polarizations along with a high polarization difference. Passive microwave measurements can be used to detect inundation [Gid-

dings and Choudhury, 1989; *Sippel et al.*, 1998]. Active instruments measure low backscattering coefficients over water surfaces. Over water, both passive and active microwave measurements are sensitive to the wind-induced surface roughness.

Microwave emissivities and backscattering coefficients are also sensitive to soil moisture. Recent investigations include studies by *Lakshmi et al.* [1997], *Owe et al.* [1999], and *Vinnikov et al.* [1999] for passive microwaves. From comparisons with in situ soil moisture measurements in Illinois, Vinnikov et al. demonstrate that passive measurements around 19 GHz show some degree of correlation with soil moisture in regions with grass and crops where the vegetation is not dense. Lakshmi et al. reach the same conclusion using simulated soil moisture. *Wagner et al.* [1999b] analyze the sensitivity of ERS scattering measurements to soil moisture in the Canadian prairies. However, soil roughness and presence of vegetation are serious challenges for the detection of soil moisture variations. While several in situ measurements of land surface emissivities and backscattering coefficients have been conducted, they do not cover the large diversity of surface types on the globe, and extrapolation from small-scale measurements to satellite field of view is not trivial.

3.3. Presentation of Monthly Maps

Plate 1 presents monthly values of NDVI (AVHRR), emissivity polarization differences, at 37 GHz (SSM/I), and scatterometer backscattering coefficients at 5.25 GHz (ERS-1) for August 1992, along with the vegetation classification map for 10 classes. There are qualitative correspondences between the three types of observations and the vegetation classification.

Desert areas (V9) are characterized by low NDVI, large emissivity differences, and low backscattering coefficients, and are clearly noticeable on each map. Variations of the backscattering coefficients and the emissivities over desert areas are interpreted in terms of rock/sand types and topography. Higher values of backscattering and lower values of emissivity polarization differences are found over high topography in the desert (Tibesti and Air in the Sahara).

Tropical rain forests display large backscattering coefficients and negligible emissivity polarization differences. However, the tropical rain forest in Africa shows rather low NDVI values compared to the rain forest in South America. Grassland and woodland are also distinguished in Africa and in South America. The sharp gradient southward of 15°N in Africa, observable on all the maps, corresponds to the Sahelian transition between arid shrub grassland and more humid grassland with tree cover.

Water surfaces (lakes, rivers, and wetlands) show high emissivity polarization differences at 37 GHz. The major river systems (e.g., Congo and Amazon) and wetlands (e.g., Pantanal in South America) appear clearly in the microwave emissivity map while they are not easily detectable in the NDVI or in the backscattering coefficient maps. With the ERS-1 scatterometer operat-

ing at 5.25 GHz, one would expect less absorption by vegetation than at the higher SSM/I frequencies and a stronger contribution from the underlying surface. The opposite is observed. See section 5.2.3 for further discussion about this signature.

4. Potential of the Satellite Data Sets for Vegetation Monitoring

4.1. Distinguishing Major Vegetation Classes

Figure 1 shows histograms of the different observations for four major vegetation types in areas in the Northern Hemisphere where the cultivation intensity is ≤20%. Evergreen and deciduous forests have been grouped together because during summer months no significant differences are observed; the same is done for woodland. As described above, the analysis is expanded beyond the parameters commonly investigated for vegetation studies (NDVI and emissivity polarization differences) to include an examination of individual channel responses. For a given observation the histograms are normalized to have the same area, giving an estimate of the probability distribution function.

From separate AVHRR channel information (VIS or NIR), only two classes of vegetation appear to be distinguishable, and even these have substantial overlap in reflectance distributions. Because absorption by chlorophyll decreases with the amount of photosynthetically active material in the vegetation, the visible reflectance is lower for grassland than for woodland and forest, as expected. Lower reflectances could also be interpreted in terms of larger fractional coverage by bare soils which have higher VIS reflectances. There is more variability in the NIR than in the VIS. Both the VIS and the NIR signals saturate for higher biomass density: it is not possible to distinguish between woodland, forest, and rain forest, based simply on a month's data. Combining those two pieces of information in the NDVI helps differentiate woodland from forest, but rain forest and other forests still appear very similar. Other authors also observed saturation of the NDVI response for high green-leaf density [e.g., *Tucker et al.*, 1985]. There are two peaks in the woodland histogram for the NDVI (also seen on the VIS histogram) with the lower value peak corresponding to arid East Africa.

For SSM/I, vegetation information is similar at all frequencies. Separating vegetation via individual SSM/I channels (vertical or horizontal polarization) cannot be done. The emissivity in horizontal polarization is lower for grassland than for tree-covered areas. With decreasing vegetation density the contribution of bare soil surfaces within a pixel increases, reducing emissivity in the horizontal polarization. The emissivity in vertical polarization shows little variation: emissivities are slightly lower for rain forest than for other forests regions, which may be explained by the large water volume in big leaves inducing significant scattering or by interception of rain droplets by the leaves. However, given the absence of in situ radiometric measurements over rain forest, these hypotheses cannot be confirmed.
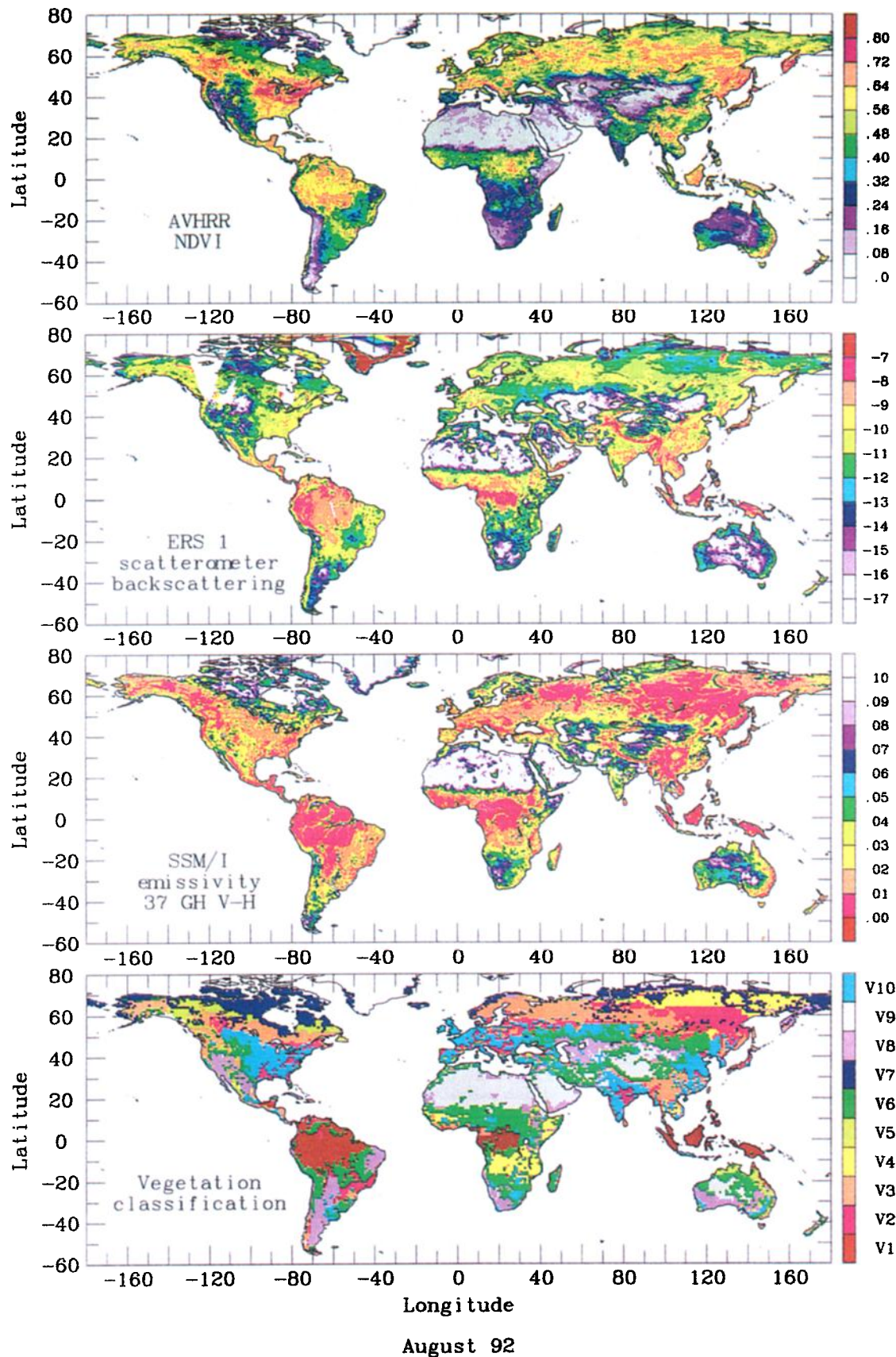
August 92

Plate 1. August 1992 monthly satellite products presented on an equal-area grid of 0.25° × 0.25° at the equator. Top to bottom: NDVI (AVHRR) from the Pathfinder, emissivity polarization differences (vertical-horizontal) at 37 GHz from SSM/I, ERS-1 scatterometer backscattering coefficient in decibels, and simplified version of the *Matthews* [1983] vegetation classification (10 classes) at a spatial resolution of 1° × 1°.
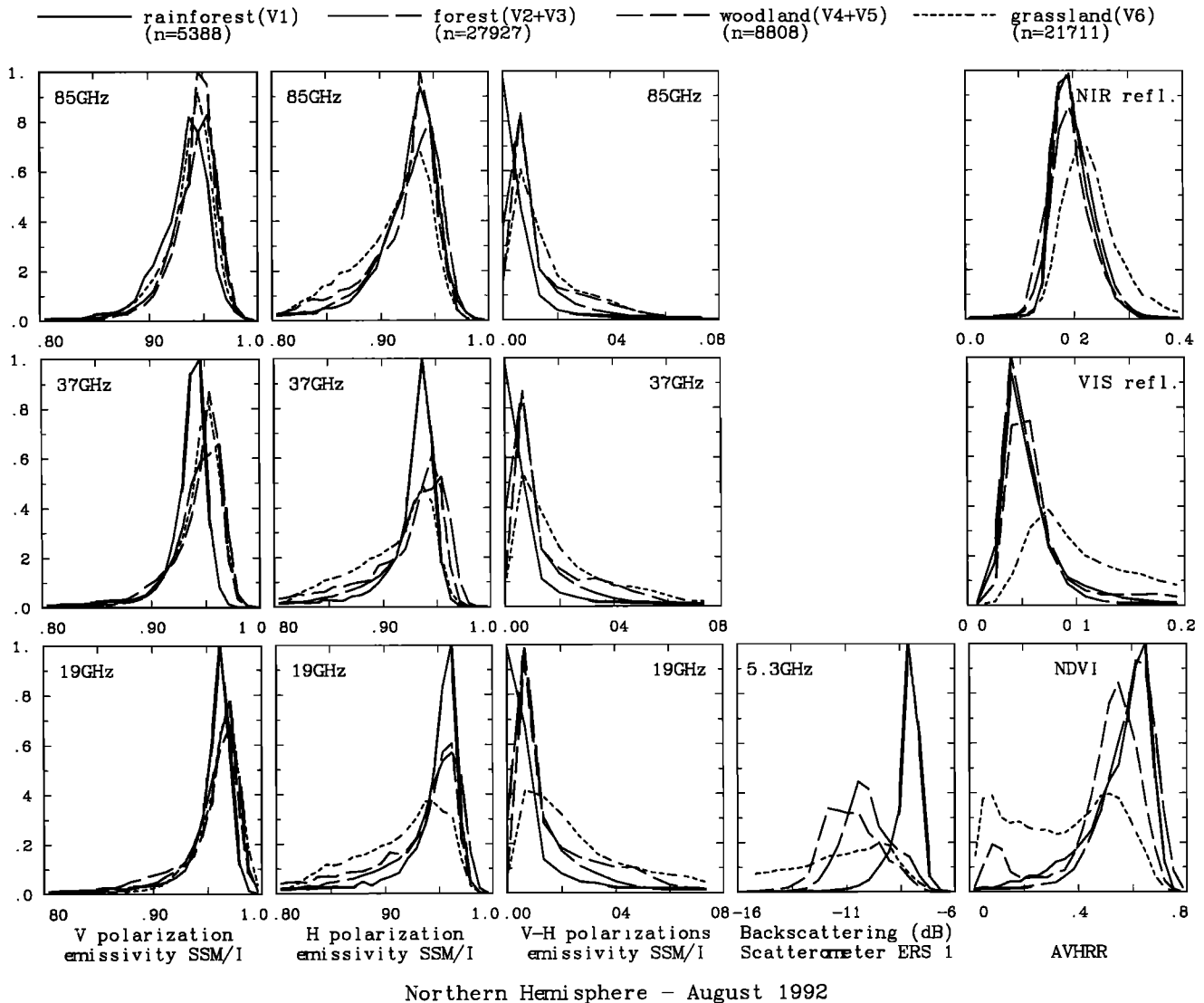
Figure 1. Histograms of the different observations for four major vegetation types, for the Northern Hemisphere. For a given observation, histograms are normalized to have the same area. Evergreen and deciduous forests have been grouped, as well as evergreen and deciduous woodlands. Only pixels with cultivation intensity ≤20% are considered. The number of pixels is indicated.

The emissivity polarization difference helps distinguish rain forest from forest/woodland and from grassland. Nevertheless, discrimination between forest and woodland is not possible.

With increasing vegetation biomass the backscattering signal from ERS-1 increases and the four histograms are rather well separated, although grassland shows a broad histogram, and overlap occurs between forest and woodland. Given the estimated error of 5%, a ~4 dB range between the peaks of tree-dominated classes represents a significant vegetation signal that is promising for discrimination of vegetation density gradients. The grassland backscatter histogram is wide as it is for all other observations (except for emissivity in vertical polarization). Grassland shows two peaks in the NDVI: the peak with high NDVI values corresponds to more humid grassland with partial tree cover, while the other

peak represents more arid grasslands with less tree cover or with shrub cover (see the 31-class vegetation classification in Table 1). By the same token, forest and woodland classes may also contain partial coverage by grassland, which might explain the difficulty of separating the grassland and the woodland/forest classes. Similar results are obtained in the Southern Hemisphere but with more confusion between forest and woodland.

4.2. Detecting Vegetation Phenology

Histograms of Northern Hemisphere observations for six vegetation types for three months corresponding to different vegetation stages are shown in Figure 2. Locations where cultivation occupies more than 20% of the cell are excluded as well as pixels that are snow covered for at least one of the three months. The snow cover in-

formation comes from the NOAA operational analysis. The mean difference between August 1992 and February 1993 is given, along with its standard deviation.

Rain forests have a stable signature in time for both passive and active microwave observations, for all months. NDVI responses over rain forest are variable, especially in the Southern Hemisphere (not shown). This seasonal variation was also reported by *Tucker et al.* [1985] for Africa, who explain their findings as due to the specific ecology of the African rain forest compared to the other rain forests elsewhere. However, the fluctuations in Figure 2 can more probably be attributed to contamination by atmospheric features such as water vapor and clouds. *Gutman* [1999] argues that over rain forest the NDVI decreases with local zenith angle, driven by a decline in the NIR due to water vapor absorption. High frequency of cirrus contamination over the tropics is also likely to induce spurious NDVI variability. Figure 3 presents scatterplots of VIS and NIR reflectances, NDVI, and radar backscattering versus the high cloud amount from ISCCP, for a $6° \times 6°$ area in the African rain forest ($3°S\ 3°N;\ 17°E\ 23°E$) for a year. NDVI and VIS reflectances show unexpectedly large variances over the year that are linearly correlated to the amount of high-clouds. No such correlation is found with the NIR and the radar signals, ruling out a possible correlation between high cloud amount and vegetation characteristics.

With microwave measurements (emissivity polarization difference and radar backscattering), responses are more stable throughout the year for evergreen forests (V3) than for deciduous ones (V2) as expected. In tree-covered regions the emissivity polarization difference stays low even in winter, and backscattering coefficient remains high. Interaction between the microwave signal and the vegetation is not limited to green leaves in the canopy but includes scattering and emission/absorption by woody parts comprising the macrostructure of the canopy. NDVI or individual VIS and NIR channels do not distinguish the two forest types: differences in the histograms for these three months are about the same for deciduous and evergreen forests, and surprisingly, the deciduous forest has the same signature in August and December.

Especially for grasslands, seasonal variations in the NDVI are predominantly due to variations in the NIR and not in the VIS. Changes in the VIS channel are small over the year and are of the order of the measurement noise. For the NIR, seasonal changes are larger, but they have similar range for all vegetation types except rain forest. As discussed by *Gutman* [1999], solar zenith angle variations can be partly responsible for the seasonal cycle of the reflectances. Water vapor variations can also modulate the signals. *Justice et al.* [1991] observed that water vapor absorption in the NIR channel may drive part of the NDVI seasonal variation, especially over grassland. *Tanré et al.* [1992] show that for grassland over Mali, correcting the NDVI from water vapor contamination can increase it by 0.1 for wet days. C. Brest at NASA Goddard Institute for Space Studies

(GISS) (personal communication, 2000) also performed a water vapor correction to AVHRR data and observed a change of $\sim$0.05 in reflectances over tropical land areas. Water vapor induced change in the NDVI is modulated by the water vapor amount, the geometry of the observation, and the surface reflectance itself: simple correction of the NDVI values cannot be easily implemented, and a full treatment of the water vapor absorption is a requirement for adequate interpretation of the reflectances in terms of surface properties only.

Individual passive microwave channels are not able to capture the seasonal cycle of any vegetation type, and mean differences between maximum and minimum in the vegetation cycle is within the noise level ($\sim$ 0.013). However, both the emissivity polarization difference and the backscattering coefficient show realistic variations within the year that can be attributed to vegetation seasonality, although the magnitude of the microwave seasonal response is small, especially for the passive measurements.

4.3. Ability to Distinguish Between Vegetation Subclasses

The different distributions of forests and woodlands (see Table 1) are physiognomically driven by climate, and, as a consequence, differences in the signals are not expected from, for instance, tropical and temperate evergreen needle-leave forests. That has been verified but is not shown here.

Separability between broad-leaved and needle-leaved tree-covered areas is very difficult to assess because the two leaf types exist in different climate regions. For instance, evergreen broad-leaved woodland (v13) is concentrated in coastal regions in Australia, while evergreen needle-leaved woodland dominates in Canada above 50°N. Attributing small signature differences exclusively to leaf type is misleading, given the large climatological differences between the two regions.

The grassland subclasses (classes 23 to 29 in the 31-class classification) represent graduations in precipitation which translate into variations in biomass density that have different signatures in the observations. Figure 4 shows time series of three grassland types v23 to v25 which represent grassland with decreasing tree and shrub cover in the two hemispheres (see Table 1). With increasing aridity and decreasing woody coverage, biomass density is lower and one expects to observe (1) increasing values of the polarization emissivities for passive microwave, (2) reduced backscattering signal for radar, and (3) lower NDVI values especially during dry months. In the Southern Hemisphere, these patterns are apparent. However, in the Northern Hemisphere, differences between v23 and v24 are opposite to what is expected for all instruments. In these areas of low vegetation density, changes in soil moisture can affect the microwave observations [e.g., *Lakshmi et al.*, 1997; *Vinnikov et al.*, 1999; *Owe et al.*, 1999]. If only the microwave observations had an unexpected behavior, variations in soil moisture could be suspected. On the contrary, the NDVI also does not show the antic-
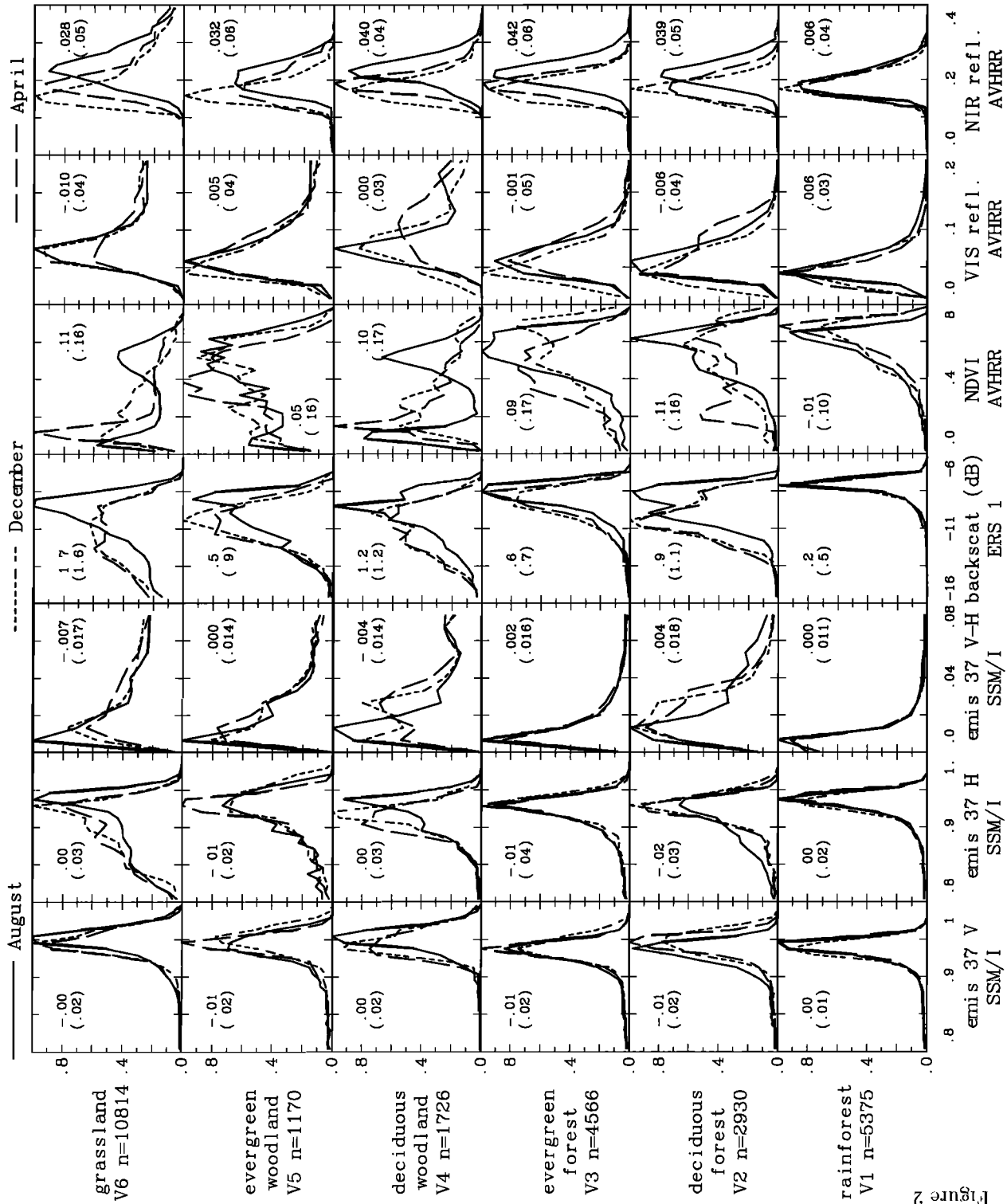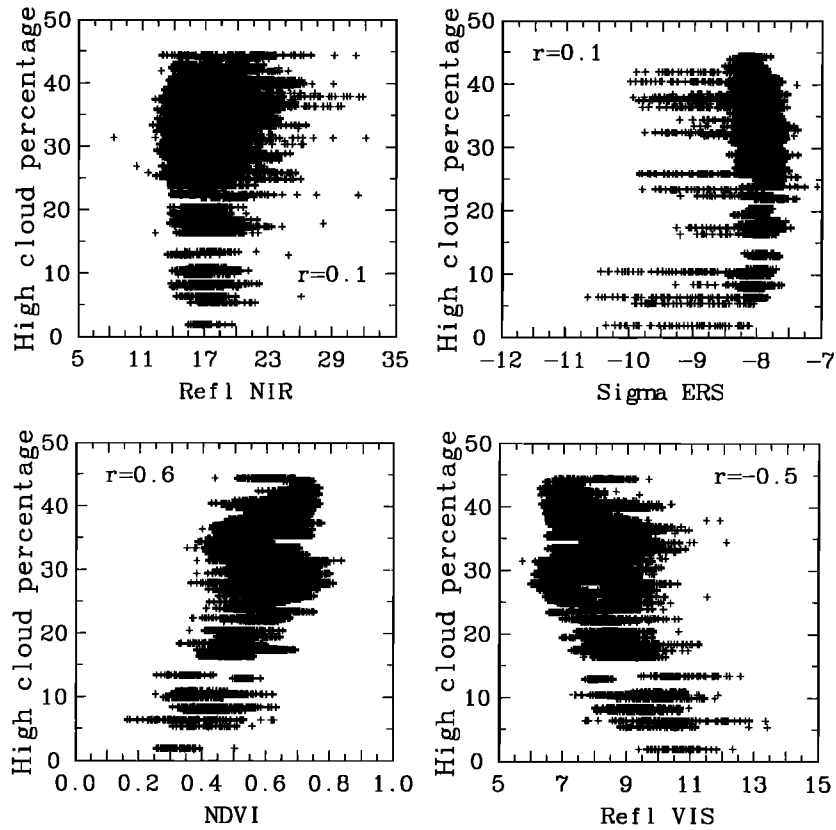
Figure 2

Figure 3. Scatterplots of NDVI, VIS, and NIR reflectances, and radar backscattering versus the high cloud amount derived from ISCCP, for a 6° × 6° area in the African rain forest (3°S 3°N; 17°E 23°E) for a year. The correlation coefficient is indicated.

ipated response and the vegetation classification may be questioned. Differences between classes 26 to 28 are related to grassland height from tall to short grassland, which should correspond to decreasing vegetation density: the expected responses are observed with all the measurements (not shown) but encompass substantial scatter. The vegetation classification should be revisited in the light of these satellite measurements, especially in Africa where land use practices may not be well documented and where anthropogenic modification of the vegetation on short timescales is occurring.

4.4. A Case Study: The Desert/Rain Forest Transition in Africa

Values of NDVI, ERS-1 backscattering, and SSM/I emissivity polarization differences (Figure 5) are compared for August and February along a cross section at longitude 20°E that encompasses a strong north-south gradient of vegetation, from the desert in Chad (lati-

tude 20°N) to the rain forest in the Democratic Republic of Congo (latitude 0°N). In this region the vegetation phenology is driven by rainfall, with an increase in the rainy season duration and in the amount of precipitation from north to south. For specific sites along the cross section the annual cycle of the three observations are presented along with the precipitation cycle as given by the Global Precipitation Climatology Project from merged infrared and microwave satellite data and gauge measurements [*Huffman*, 1996]. The vegetation type is indicated as given by *Matthews* [1983] 31-type classification. All the variables are normalized for an easier comparison (see the figure caption).

North of 16°N the three observations are stable in time, with low NDVI values and high emissivity polarization differences. The backscattering signatures change abruptly between 17°N and 18°N: around 17°N, sand dunes induce a very low backscattering signature because of volume scattering in sand, whereas north

Figure 2. For the Northern Hemisphere and for the different observations, histograms of six vegetation types, for three months that correspond to different vegetation stages. Areas where the cultivation intensity is ≥20% are excluded, as well as pixels that are snow covered for at least one month. The number of pixels is indicated. Numbers indicate the mean difference between August 1992 and February 1993, along with the standard deviations in parenthess.
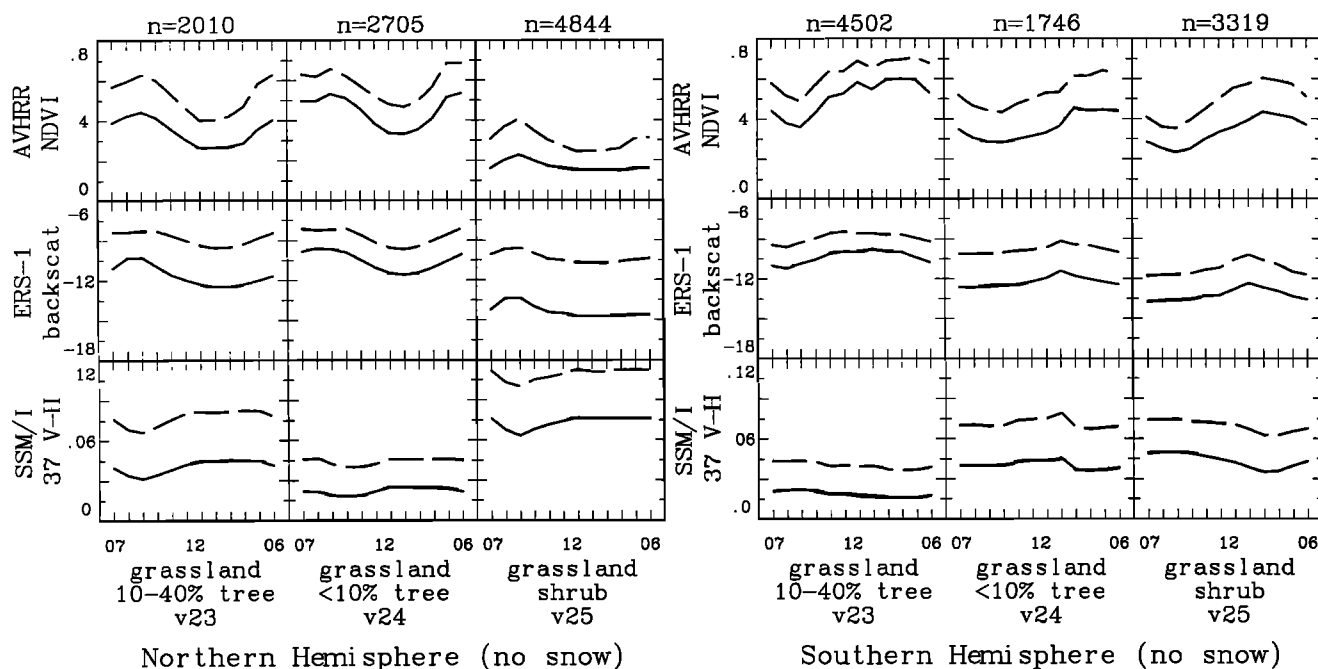
Figure 4. For three grassland types with different woody cover, time series over a year (July 1992 to June 1993) of the mean response (solid lines) of three selected observations (AVHRR NDVI, ERS-1 scatterometer backscattering coefficient in decibels, and SSM/I emissivity polarization difference at 37 GHz). The standard deviation is also plotted (dashed lines). Pixels that are snow covered for at least one month during the year are excluded. Results are presented for the Northern and Southern Hemispheres, and the number of pixels is indicated.

of 18°N, the backscattering signal increases with the presence of rocks [*Food and Agriculture Organization (FAO)-UNESCO*, 1977].

South of 16°N, differences between summer and winter increase for all observations. From (16°N, 20°E) to (6°N, 20°E) the seasonal cycle of the various grassland types (from classes 23 to 25) is well captured by the three types of observations, and the observations vary in phase. Vegetation, associated with the rainy season, develops rapidly as soon as the rainy season starts, followed by a slow decline during senescence. *Frison et al.* [1998] analyzed the relative contributions of soil and vegetation in a case study in a semi-arid environment in Northern Sahel (Mali), concluding that although the soil component is always large, the backscattering coefficient reflects vegetation development well. As expected, passive and active microwave responses are very stable for rain forest (see the annual cycle at 1°N, 20°E). However, for the same area, NDVI exhibits large and rapid

fluctuations during the year that cannot be explained by vegetation phenology.

At several locations along the cross section the SSM/I response shows large declines in the emissivity polarization differences, especially in August during the rainy season. At 10°N, for instance, the decrease in emissivity polarization difference is related to the Slamat swamps in Chad. The decline around 13°N could be related to swamps around the Batha River in Chad, but that should be further investigated. Around 2°N in the rain forest the Congo River and its associated swamps induce a decrease in the emissivity polarization. There are no significant changes in the backscattering coefficient nor in the NDVI.

4.5. Correlation Between the Three Types of Observations

Figure 6 represents the scatterplots of all possible pairs of observations, for the NDVI, the backscattering

Figure 5. Comparisons of AVHRR NDVI, ERS-1 backscattering coefficient, and SSM/I emissivity polarization difference at 37 GHz along a cross section at 20°E from 20°N to the equator, for August 1992 and February 1993. The vegetation class in *Matthews* [1983] classification is indicated for each degree. For five specific sites along the cross section the full seasonal cycle is given with the precipitation rate in mm.d^{-1} extracted from the Global Precipitation Climatology Project data set. For comparison purposes, all the values are linearly normalized between 0 and 1 that correspond to variations from 0 to 1 for the NDVI, from -26 to -6 dB for the ERS-1 backscattering coefficient, from 0.15 to 0.0 for the SSM/I emissivity polarization difference, and from 0 to 12 mm.d^{-1} for the rain rate.

(for each degree, class in Matthews classification)
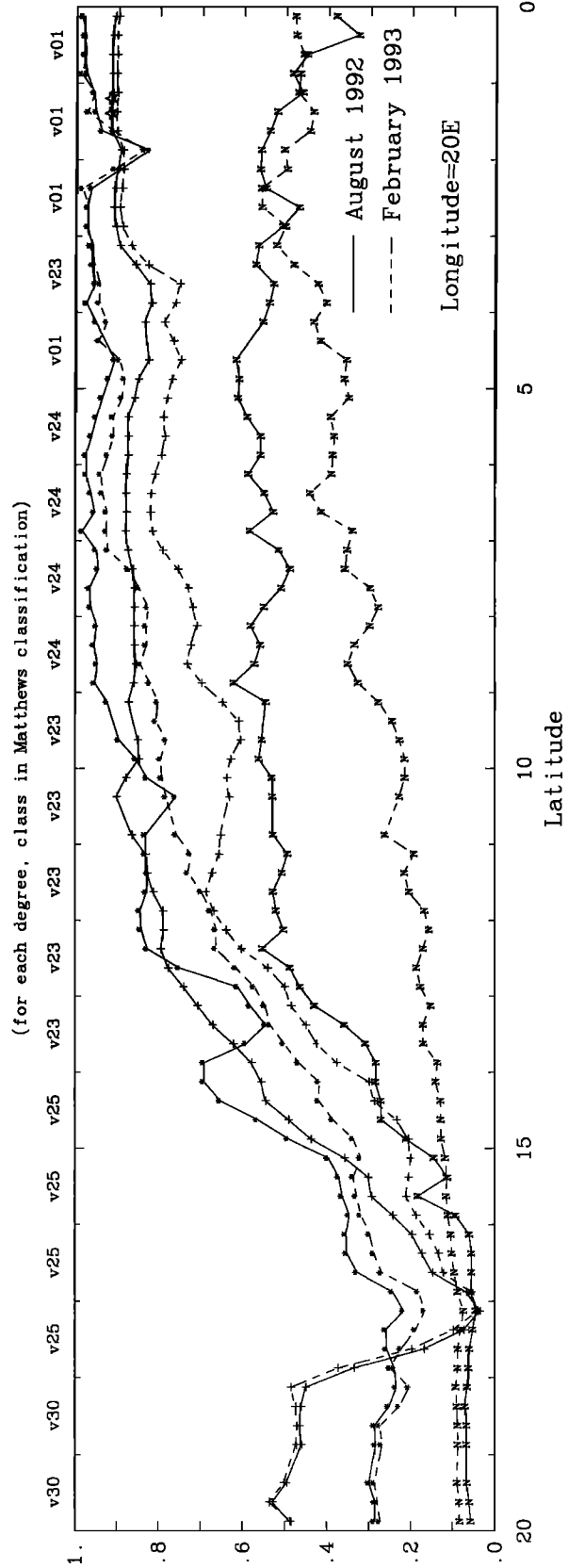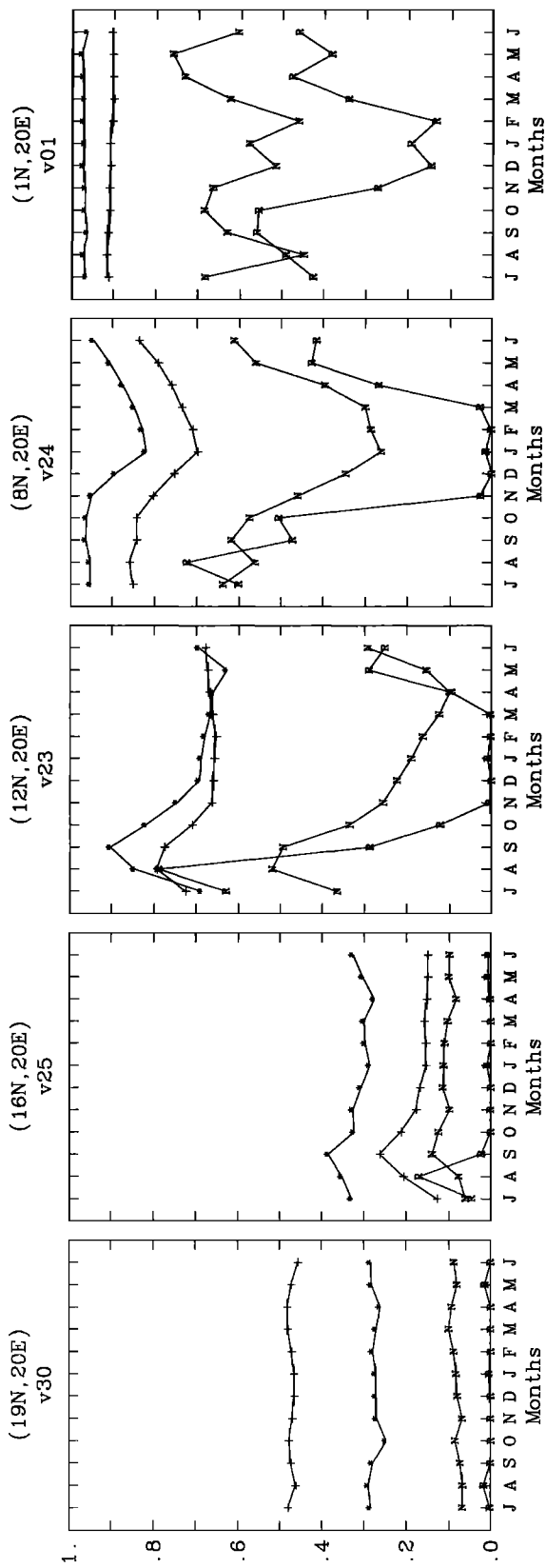
N AVHRR NDVI;   + ERS-1 backscattering coef;   * SSM/I emissivity V-H 37 GHz;   R rain in mm/day (GPCP)
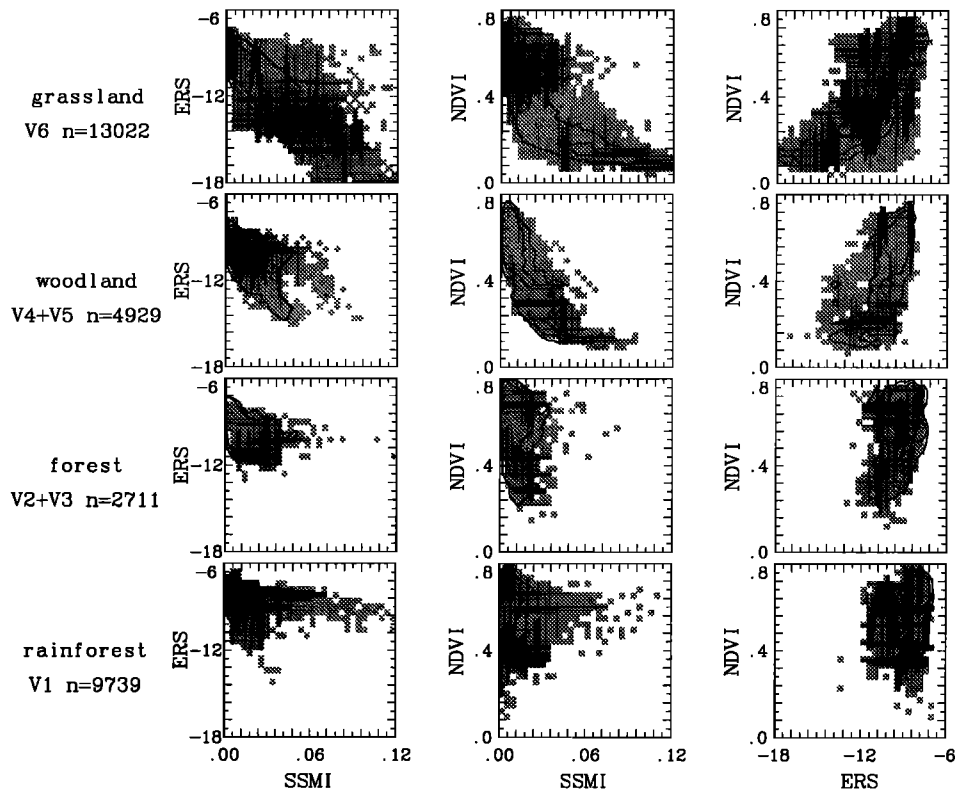
Figure 6. Scatterplots of all possible pairs of observations for the AVHRR NDVI, the ERS-1 backscattering coefficient, and the SSM/I emissivity polarization difference at 37 GHz for four major vegetation types. Results are presented for the Southern Hemisphere during summer (February 1993). For each scatterplot the population contours at 0.5% and 0.2% are drawn.

coefficient, and the emissivity polarization difference at 37 GHz, for four major vegetation types in South America in August. For each scatterplot the population contours at 0.2% and 0.5% are drawn.

For the rain forest the ERS backscattering coefficients show little dispersion, whereas the NDVI and the emissivity polarization difference exhibit larger scatter. For the NDVI, atmospheric contaminations are suspected. Pixels with large emissivity polarization differences (≥ 0.01) are concentrated in coastal areas and around the major river systems (Congo in Africa and the Amazon in South America), confirming high sensitivity of the passive microwave measurements to water surfaces compared to the other measurements. ERS-1 backscattering signal shows more dynamic range than SSM/I in densely vegetated areas outside wet areas, with population contours elongated along the backscattering coefficient axis. For emissivity polarization differences between 0.00 and 0.02, ERS backscattering coefficient varies between ~-7 and ~-12 dB over forest and woodland, with lower values of the backscattering coefficients corresponding to the transition zones between forest/woodland and grasslands. ERS-1 radar signal has the ability to detect density gradients in forested areas.

5. Integrated Analysis of Spectral Variations With a Clustering Technique

5.1. Description of the Clustering Technique

In the preceding sections we analyzed the response of individual spectral bands to various types of vegetation. We also examined relationships between pairs of spectral observations. A clustering technique has been developed to integrate all the data sets to obtain an analysis of the variations of one spectral band with respect to the others. At this stage the clustering technique is a tool to interpret the variability of the data and is not yet optimized for vegetation classification.

Let $\{X^i \in R^n \; ; \; i = 1, \ldots, M\}$ be an observational data set, where n is the dimension of the observation (i.e., the number of channels in the following) and M is the number of observations (i.e., the number of monthly pixels). The goal of unsupervised classification algorithms is to classify data sets into subgroups that optimally describe the statistical variability present in the data, without any a priori information or guidance about classes. Clustering techniques define K prototypes (or clusters) P^i that discretizes the continuous observations and optimally quantify their variability.
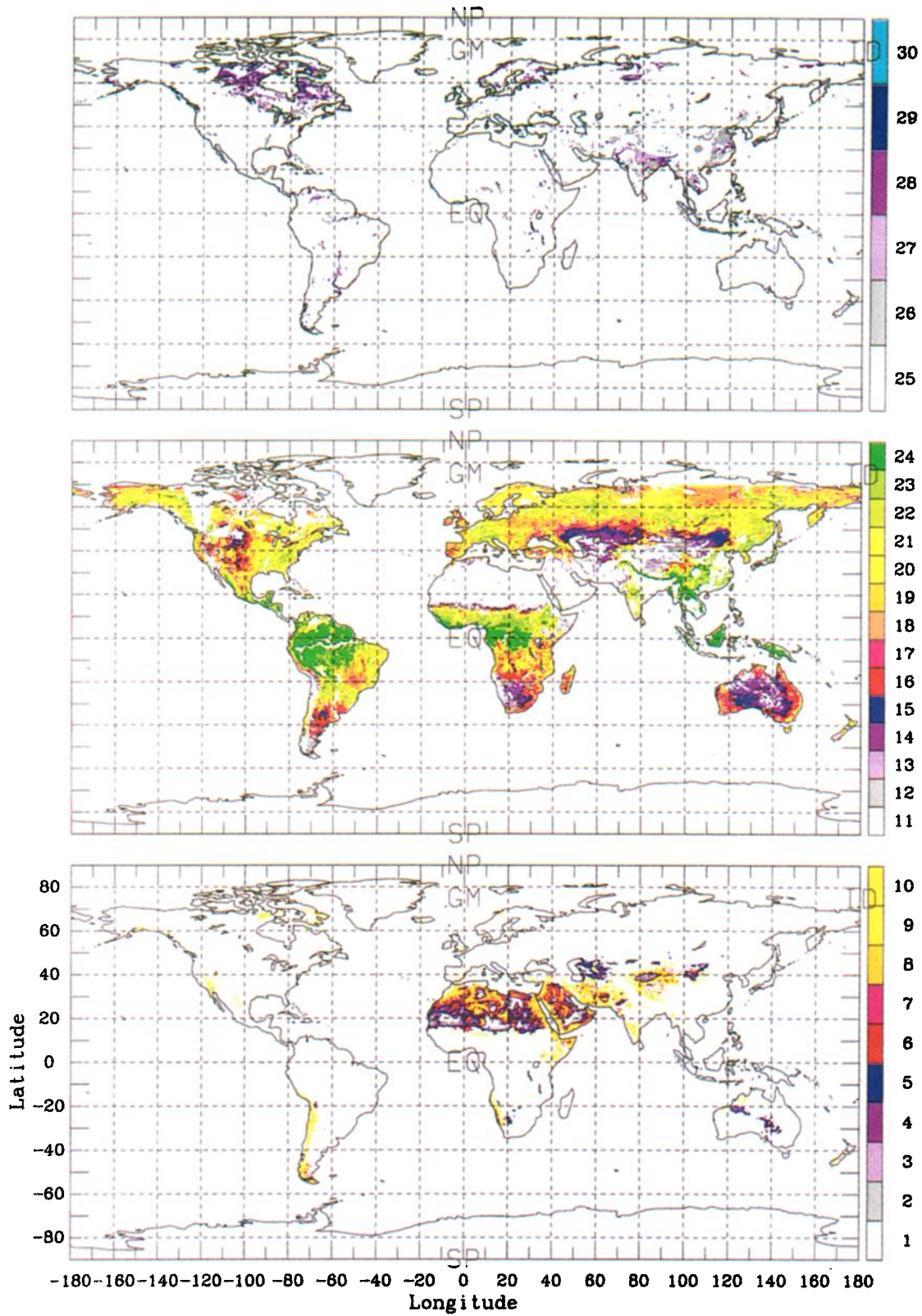
**Cluster SSMI ERS1 AVHRR
August 1992**

Plate 2. Cluster map derived from the *Kohonen* [1984] scheme for August 1992.

Each observation X^i is associated with the prototype for which the distance $d(X^i, P^k)$ is smallest.

Kohonen [1984] topological feature maps are also called self-organizing topological maps. The distinguishing feature of this algorithm is that a neighborhood requirement is imposed on the prototypes [*Schaale and Furrer*, 1995; *Aires*, 1999], so that when the algorithm has converged, prototypes corresponding to nearby points on the map grid have nearby locations in the data space. This additional information on the extracted prototypes helps interpret the prototypes. The neighborhood system adopted in this study is a one-dimensional ordering of prototypes where the neighborhood of a prototype is its two nearest neighbor prototypes. This neighborhood system is well adapted to the definition of a statistical index whose value is to describe the links and variabilities in the data set.

The *Kohonen* [1984] classification algorithm is applied to a year of monthly observations for SSM/I, ERS-1, and AVHRR ($M=12$). Each observation vector corresponds to one snow-free pixel of $0.25° \times 0.25°$ at the equator and has 13 components ($n=13$) which are (1) nine SSM/I derived variables: the emissivities for each polarization and their polarization difference at 19, 37, and 85 GHz; (2) the ERS-1 backscattering coefficient; and (3) the AVHRR NDVI and reflectances in the VIS and NIR. Each observation in the observational vector is normalized by its mean spatial variance over a year. The same weight is given to each instrument, meaning that every observation is weighted by a coefficient 1/9, 1/1, and 1/3 for SSM/I, ERS, and AVHRR, respectively. The number of prototypes K is chosen to be 30. In this study, the distance d is the absolute value of the difference; compared to the traditional Euclidian distance, it gives less weight to potential outliers.

5.2. Results of the Clustering and Joint Analysis of the Spectral Bands

The *Kohonen* [1984] algorithm is applied to estimate the $K = 30$ clusters, P^k, that optimally quantify the data set. Upon convergence of the algorithm, each observation X^i is associated with its closest prototype using the distance d. A cluster map is produced for each month; Plate 2 shows the results for August 1992. Figure 7 represents the $n = 13$ coordinate values (i.e., the channel observations) of each prototype P^k with respect to the cluster number, from cluster 1 to cluster $K = 30$. The standard deviation of the subgroup of observations associated with each prototype is added to the figure. It is a measure of the dispersion of the observations in a subgroup. For a prototype a low standard deviation in a channel means that the channel provides good discriminant information in the clustering solution: the relationship between the cluster and the channel is not ambiguous. On the other hand, a high standard deviation means that the prototype is relatively insensitive to that channel. High standard deviations can origi-

nate from instrumental noise, from spatial heterogeneity within single pixels, or from variability that contaminates the channel but is not related to the surface properties (e.g., atmospheric contamination).

The number of prototypes K was chosen so that, for each prototype, at least one of the channels provides statistical discrimination: for this channel the difference between the two consecutive prototypes is above the standard deviation of subgroups associated with each prototype. The ambiguity between prototypes is thus minimized. As a consequence, each class shows good spatial consistency on the maps. The variability in each cluster subgroup, which depends on the value and the number of observations in the subgroup, is uniformly distributed by the *Kohonen* [1984] algorithm in each prototype for an optimal quantification of the data set.

The 30 clusters have been separated into three major cover types (see Plate 2): (1) arid environments (clusters 1 to 10), (2) vegetated areas (clusters 11 to 24), and (3) wet regions (clusters 25 to 30). Clusters 11 to 24 can be compared to a vegetation density gradient that shows similarities with *Matthews* [1983] vegetation classification. Although it is not our purpose here to classify the vegetation, a quick comparison is performed between the clustering results and Matthews' classification for the Northern Hemisphere in August. 58% of class V1 (rain forest) in Matthews' classification correspond to cluster 24, and 17% are in cluster 25. Forest types (V2+V3) have their maximum populations in cluster 21, while woodland (V4+V5) is concentrated in cluster 19.

5.2.1. Arid environments. Clusters 1 to 3 correspond closely to sandy deserts [*FAO-UNESCO*, 1977] with high reflectances in the VIS and NIR, low backscattering signals from ERS-1, and large polarization differences for SSM/I. Clusters 4 to 8 have similar VIS and NIR reflectances, while the backscattering signal increases by ~9 dB due to increasing surface roughness related to the combined effects of rocky surfaces and topography. SSM/I polarization differences decrease with surface roughness. Clusters 9 and 10 correspond to desert areas in high topography, and they show a large backscattering signal compared to the surrounding areas. Radar signals have a high sensitivity to surface roughness that could be used to characterize desert properties, especially in the context of estimating dust sources [*Marticorena et al.*, 1997].

5.2.2. Vegetated areas. The cluster numbers between 11 and 24 could be linearly transformed into a multivariate-source index related to vegetation density. Clusters 11 to 13 are predominantly located in arid areas. From cluster 14 to 24, NDVI, radar backscattering, and the microwave polarization differences show a smooth increase corresponding to increasing vegetation density. Changes in the backscattering signal amount to 6 dB, which is very significant compared to the 5% accuracy of the measurement. In addition, the backscattering standard deviation is very low for these clusters,
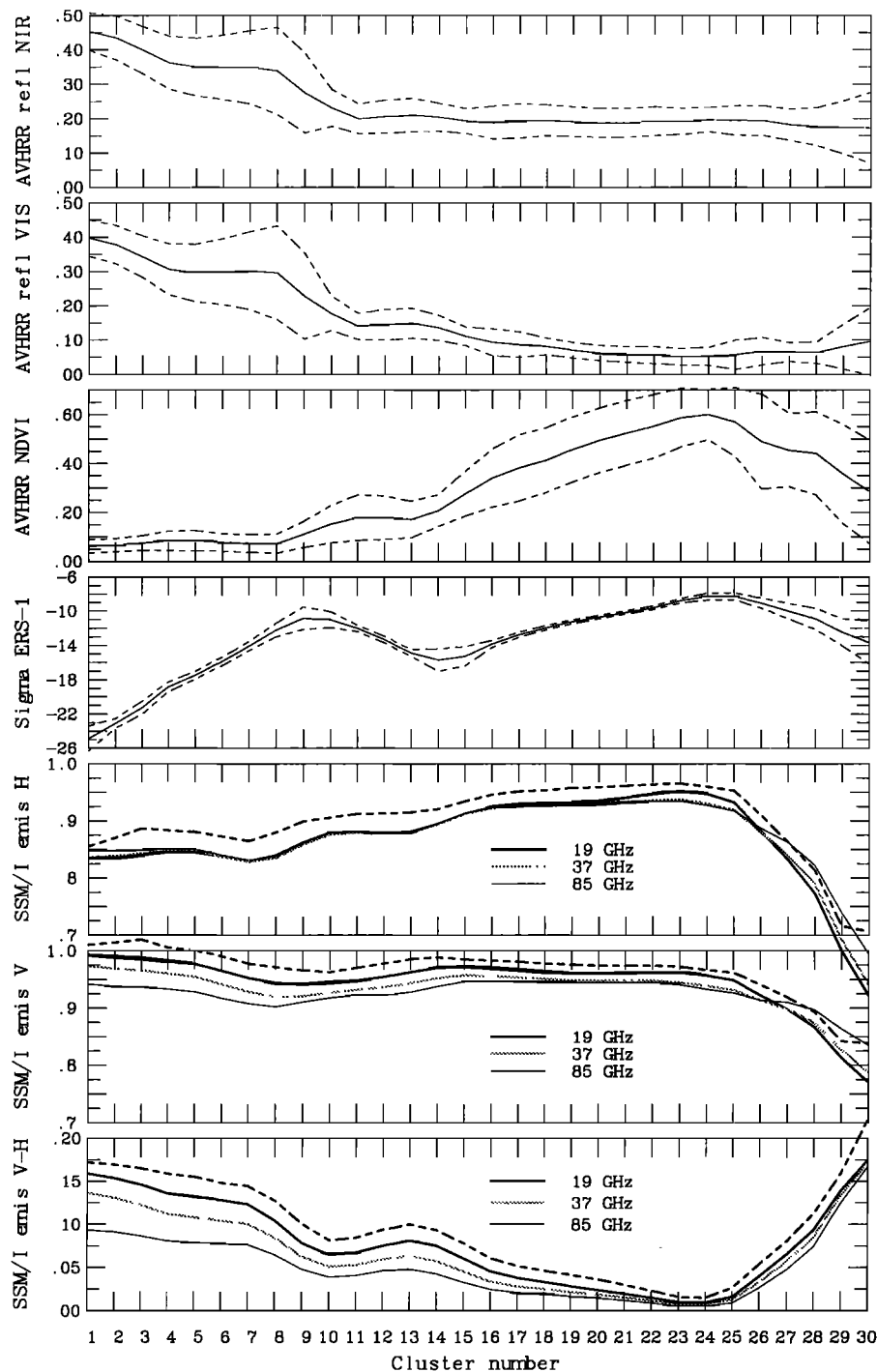
Figure 7. Value of the prototype in each cluster for each observation type (solid line), along with the standard deviation around this prototype in the cluster (dashed line). For passive microwaves, standard deviations are indicated for 19 GHz only: The standard deviations for the other channels are similar.

indicating that the radar signal is the most effective discriminator. Although NDVI increases smoothly, its large standard deviation in these clusters shows that separation between clusters is not closely related to its value. NIR does not vary much, while VIS reflectance changes from 0.15 to 0.05. In vegetated areas, emissivities in the vertical polarization decline with increasing frequency, which is contrary to model predictions. This

has already been discussed by *Prigent et al.* [2000]. In the horizontal polarization, emissivities are almost constant except for very densely vegetated areas, reinforcing the hypotheses of stronger scattering by vegetation with increasing frequency. These signatures will be further explored with the help of a radiative transfer model [*Wigneron et al.*, 1993].

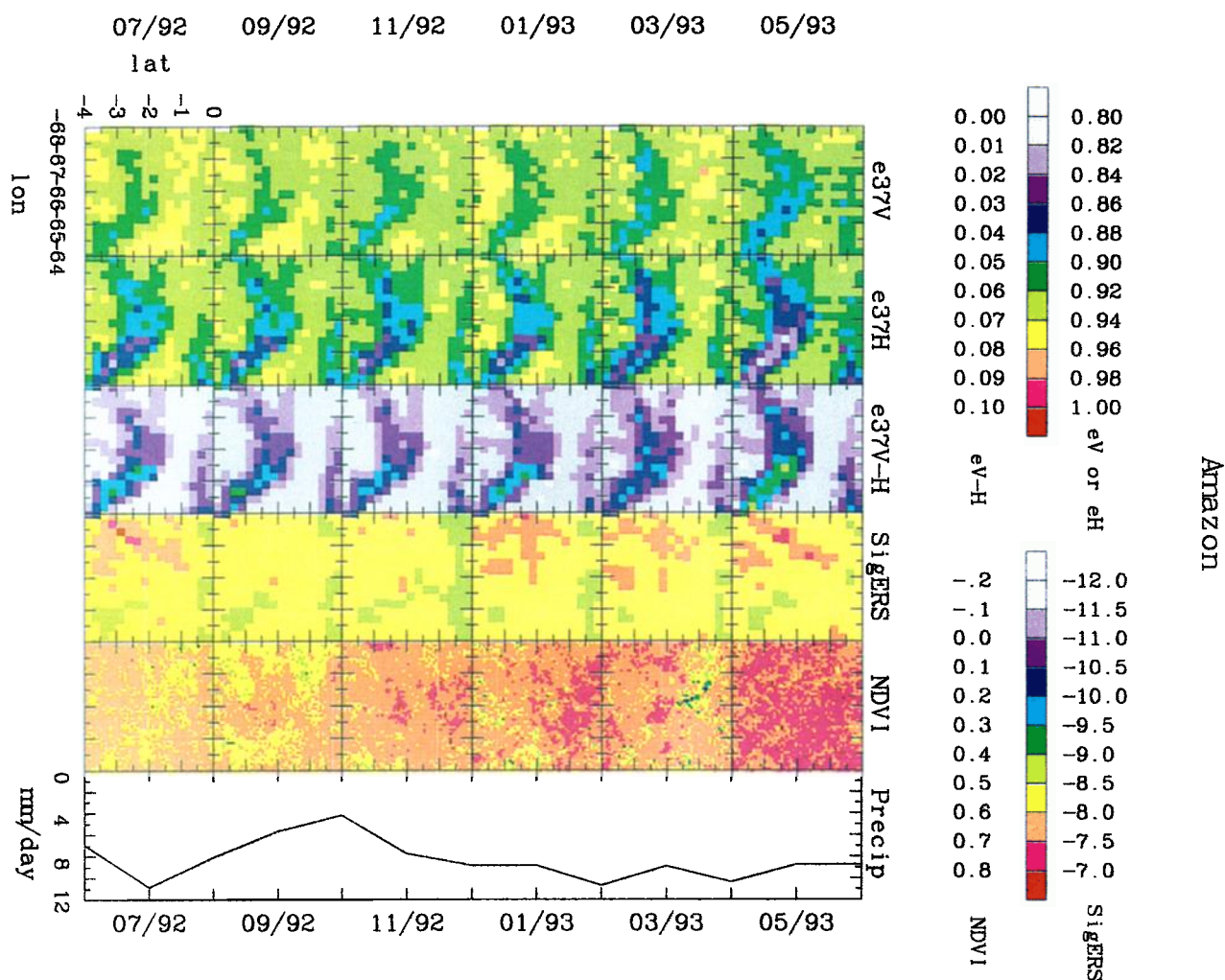**5.2.3. Wetland areas.** From cluster 25 to 30

Plate 3. Response of each instrument over wetlands in an area in the Amazon rain forest, for every other month between July 1992 and June 1993. The precipitation is also indicated as given by Global Precipitation Climatology Project.

the passive microwave signals vary substantially with rather low standard deviations, while the other variables show small changes with large standard deviations. This result confirms the high sensitivity of microwave signals to the presence of water and the potential for microwave detection of inundated areas. Plate 3 shows the response of the three instruments in the Amazonian rain forest for a year. While the passive microwave clearly detects the location and seasonal cycle of wetlands surrounding the river, the active microwave instrument does not. With increasing frequency, one expects higher attenuation and scattering by vegetation, and as a consequence a lower sensitivity to soil properties. Although operating at a lower frequency than SSM/I, ERS-1 scatterometer shows much less sensitivity to inundated areas. This suggests that scattering by the vegetation could dominate the radiative transfer processes in the canopy, exceeding the absorption/emission contribution within the vegetation. However, complex physical interactions take place between the soil surface and the canopy, and further investigations have to be conducted. Unified radiative transfer

models are now capable of simulating both the emissivity and the backscattering responses of vegetation and soil [*Wigneron et al.*, 1993; *Karam et al.*, 1995]. Using a radiative transfer model at 1.5 GHz, *Du et al.* [2000] attempt to assess which of the two sensing techniques (passive or active) is less affected by vegetation cover when trying to estimate soil moisture. They conclude that the two sensor types have similar sensitivity to vegetation. Joint analysis of the emissivity and backscattering model responses, compared to ERS and SSM/I observations, will help better understand the vegetation and soil interaction with the microwave radiation.

6. Conclusion

This study presents a global evaluation and comparison of measurements in the visible and near-infrared, as well as passive and active microwave observations for characterizing vegetation cover and seasonality. It is the first step toward global characterization of the land surface using multisatellite observations comprising a large spectral range. A year of monthly observations of

AVHRR (NDVI, visible, and near-infrared reflectances), SSM/I (emissivities between 19 and 85 GHz), and ERS-1 (wind scatterometer backscattering coefficients) was analyzed with a spatial resolution of $0.25° \times 0.25°$ at the equator. The capacity to discriminate various vegetation types is assessed in the context of the *Matthews* [1983] vegetation classification, with special emphasis on the ability to detect vegetation phenology and density. A clustering technique derived from the *Kohonen* [1984] topological maps is developed to integrate observations from all three instruments and to provide a synthesis of the sensitivities of the suite of spectral bands to surface properties.

NDVI varies from ~ 0.1 to ~ 0.7 in response to vegetation density with an estimated error of 0.1; the index saturates in forested areas. The NDVI has a marked seasonal cycle for most vegetation types that is mostly driven by changes in the near-infrared reflectances, not by variations in the visible reflectances. Time series over evergreen vegetation show spurious seasonal variations of up to 0.2 in the NDVI. Significant cirrus contamination is apparent over the African tropical forest. Atmospheric contamination (clouds, water vapor, and aerosols) and solar zenith angle dependences also alter the signal. A full correction for atmospheric contamination of the AVHRR VIS and NIR reflectances is required in order to interpret the reflectances and/or NDVI in terms of vegetation only. This task has been undertaken at NASA GISS. Understanding spatial and temporal variations in the VIS and NIR reflectances is of primary importance for the interpretation and prediction of the surface albedo, which is a key parameter in the Earth energy budget.

Passive and active microwave observations respond to the absorption/emission and scattering by vegetation elements including woody parts and are not directly sensitive to the photosynthesis activity. These measurements therefore complement the AVHRR observations by indicating structural density.

Active microwave backscattering observations (ERS-1) are not affected by variations in atmospheric conditions and do not require significant preprocessing. Measured with an accuracy of 5%, backscattering signals exhibit a high potential to characterize bulk vegetation density including green-leaf and woody structures, with ~ 10 dB changes from rain forest to arid grassland. In contrast to NDVI, they have a stable seasonal response over evergreen vegetation and show a realistic annual cycle over deciduous vegetation. In arid places, backscattering measurements are very sensitive to surface roughness and show very strong signatures over sand dunes, making them a potential tool for desert studies. Unaffected by atmospheric variability, scatterometers appear to be very promising instruments for land surface characterization, due to their high sensitivity to vegetation, as well as for their potential value in desert investigations.

This study reports on a new atlas of microwave emissivities calculated from SSM/I between 19 and 85 GHz using ancillary data to remove atmospheric contributions. Emissivity polarization differences from this data set show some ability to characterize vegetation types but exhibit a smaller dynamic range than ERS-1 observations do; values range from ~ 0.00 for tropical forests to ~ 0.08 for arid grasslands, with an estimated error of ~ 0.013. Vegetation discrimination is not possible from individual polarizations and sensitivity to vegetation does not vary substantially with frequency. However, passive microwave measurements exhibit a strong sensitivity to standing water, making it possible to detect wetlands even in densely vegetated areas. A method to detect the seasonality and extent of inundated areas is under development, using both passive and active microwave instruments; the active observations help to estimate signal attenuation by vegetation. Although operating at a lower frequency, ERS-1 scatterometer observations show much less sensitivity to inundated areas. This suggests that scattering by the vegetation may dominate the radiative transfer processes in the canopy, exceeding the absorption/emission contribution within the vegetation. Unified radiative transfer models are now capable of simulating both the emissivity and the backscattering responses of vegetation and soil [*Wigneron et al.*, 1993; *Karam et al.*, 1995]. Integrated analysis of the emissivity and backscattering model responses, compared to ERS and SSM/I observations, will help better understand the interaction of vegetation with microwave radiation.

Matthews [1983] vegetation classification is used as a land-urface reference data set in this analysis and it appears that this classification should be revisited in the light of this study, especially in transition zones and in semi-arid environments. *DeFries et al.* [1995] reviewed dominant biophysical processes and concluded that among the most important vegetation characteristics controlling biospheric fluxes are growth form (tree, shrub, and herb) and seasonality of woody vegetation (deciduous and evergreen). Our study suggests that an integrated analysis of a suite of observations from three satellite instruments may successfully characterize large-scale features of these two vegetation properties. This analysis has the added advantage of identifying wetland features which play important roles in hydrological and biogeochemical cycles. Unsupervised clustering techniques using *Kohonen* [1984] topological maps not only helped the joint interpretation of this suite of spectral data sets but also showed potential for land cover classification. From the sensitivity analysis described here, an optimal set of variables can be selected that are relevant for a variety of land cover characterizations. Further improvements of the clustering technique will include the use of observation time series for a year instead of monthly data in order to take into account the seasonal cycle of each vegetation type and the use of a priori information (altitude and latitude). Combining observations from the three instruments makes it possible to benefit from their complementary strengths to extract maximum information about vegetation biophysical characteristics on a global basis and to minimize problems related to one instru-

ment only. Such an approach should improve the ability to monitor changes with time based on series of benchmark behaviors derived from the suite of instruments.

References

Aires F., Problèmes inverses et réseaux de neurones: Application à l'interféromètre haute résolution IASI et à l'analyse de séries temporelles, Ph.D. thesis, Paris IX-Dauphine, Univ. Paris, 1999.

Asrar, G., M. Fuchs, E. T. Kanemasu, and J. L. Hatfield, Estimating absorbed photosynthetic radiation and leaf area index from spectral reflectance in wheat, *Agron. J.*, *76*, 300-306, 1984.

Bauer, K. G., and J. A. Dutton, Albedo variations measured from an airplane over several types of surface, *J. Geophys. Res.*, *67*, 2367-2376, 1962.

Begue, A., and R. Myneni, Operational relationships between NOAA-advanced very high resolution radiometer vegetation indices and daily fraction of absorbed photosynthetically active radiation, established for Sahelian vegetation canopies, *J. Geophys. Res.*, *101*, 21,275-21,289, 1996.

Choudhury, B. J., Monitoring global land surface using Nimbus-7 37 GHz data. Theory and examples, *Int. J. Remote Sens.*, *10*, 1579-1605, 1989.

Choudhury, B. J., and C. J. Tucker, Monitoring global vegetation using Nimbus-7 37GHz data. Some empirical relations, *Int. J. Remote Sens.*, *8*, 1085-1090, 1987.

Colton, M. C., and G. A. Poe, Intersensor calibration of DMSP SSM/I's: F-8 to F-14, 1987-1997, *IEEE Trans. Geosci. Remote Sens.*, *37*, 418-439, 1999.

Colwell, J. E., Vegetation canopy reflectance, *Remote Sens. Environ.*, *3*, 175-183, 1974.

DeFries, R. S., et al., Mapping the land surface for global atmospheric-biosphere models: Toward continuous distributions of vegetation's functional properties, *J. Geophys. Res.*, *100*, 20,867-20,882, 1995.

DeFries, R. S., J. R. G. Townshend, and M. C. Hansen, Continuous fields of vegetation characteristics at the global scale at 1-km resolution, *J. Geophys. Res.*, *104*, 16,911-16,923, 1999.

Deroin, J. P., A. Company, and A. Simonin, An empirical model for interpreting the relationship between backscattering and arid land surface roughness as seen with SAR, *IEEE Trans. Geosci. Remote Sens.*, *35*, 86-92, 1997.

Du, Y., F. T. Ulaby, and G. Dobson, Sensitivity to soil moisture by active and passive microwave sensors, *IEEE Trans. Geosci. Remote Sens.*, *38*, 105-114, 2000.

Ferrazzoli, P., and L. Guerriero, Passive microwave remote sensing of forest: A model investigation, *IEEE Trans. Geosci. Remote Sens.*, *34*, 433-443, 1996.

Food and Agriculture Organization (FAO)-UNESCO, Soil map of the world, 1:5M scale, UNESCO, Paris, 1977.

Frison, P.-L., and E. Mougin, Use of ERS-1 wind scatterometer data over land surfaces, *IEEE Trans. Geosci. Remote Sens.*, *34*, 550-560, 1996a.

Frison P.-L., and E. Mougin, Monitoring global vegetation dynamics with ERS-1 wind scatterometer data, *Int. J. Remote Sens.*, *17*, 3201-3218, 1996b.

Frison, P.-L., E. Mougin, and P. Hiernaux, Observations and interpretation of seasonal ERS-1 wind scatterometer data over Northern Sahel (Mali), *Remote Sens. Environ.*, *63*, 233-242, 1998.

Fung, I. Y., C. J. Tucker, and K. C. Prentice, Application of advanced very high resolution radiometer vegetation index to study atmosphere-biosphere exchange of CO_2, *J. Geophys. Res.*, *92*, 2999-3015, 1987.

Gausman, H. W., Leaf reflectance of near-infrared, *Photogramm. Eng.*, *40*, 183-191, 1974.

Giddings, L., and B. J. Choudhury, Observation of hydrological features with Nimbus-7 37 GHz data applied to South America, *Int. J. Remote Sens.*, *10*, 1673-1686, 1989.

Gutman, G. G., On the use of long-term global data of land reflectances and vegetation indices from the advanced very high resolution radiometer, *J. Geophys. Res.*, *104*, 6241-6255, 1999.

Hewison, T. J., Airborne measurements of forest and agricultural land surface emissivity at millimeter wavelengths, *IEEE Trans. Geosci. Remote Sens.*, 39, 393-399, 2001.

Holben, B. N., Characteristics of maximum-value composite images from temporal AVHRR data, *Int. J. Remote Sens.*, *7*, 1417-1434, 1986.

Hollinger, J. P., R. Lo, G. Poe, R. Savage, and J. Pierce, Special Sensor Microwave/Imager user's guide, Nav. Res. Lab., Washington, D. C., 1987.

Hollinger, J. P., J. L. Pierce, and G. A. Poe, SSM/I instrument evaluation, *IEEE Trans. Geosci. Remote Sens.*, *28*, 781-790, 1990.

Huffman, G. J., GPCP version 1 combined precipitation data set, SSAI, NASA Lab. for Atmos., Goddard Space Flight Cent., Greenbelt, Md., 1996.

James, M. E., and S. N. V. Kalluri, The Pathfinder AVHRR land data set: An improved coarse resolution data set for terrestrial monitoring, *Int. J. Remote Sens.*, *15*, 3347-3364, 1994.

Justice, C. O., J. R. Townshend, and B. J. Choudhury, Comparison of AVHRR and SMMR data for monitoring vegetation phenology on a continental scale, *Int. J. Remote Sens.*, *10*, 1607-1632, 1989.

Justice, C. O., T. F. Eck, D. Tanré, and B. N. Holben, The effect of water vapor on the normalized difference vegetation index derived for the Sahelian region from NOAA AVHRR data, *Int. J. Remote Sens.*, *12*, 1165-1187, 1991.

Kalnay, E., et al., The NCEP/NCAR 40-year reanalysis project, *Bull. Am. Meteorol. Soc.*, *77*, 437-470, 1996.

Karam, M. A., F. Amar, A. K. Fung, E. Mougin, A. Lopes, D. M. Le Vine, and A. Beaudoin, A microwave polarimetric scattering model for forest canopies based on vector radiative transfer theory, *Remote Sens. Environ.*, *53*, 16-30, 1995.

Kennett, R. G., and F. K. Li, Seasat over land scatterometer data, I, Global overview of the Ku-band backscatter coefficients, *IEEE Trans. Geosci. Remote Sens.*, *27*, 592-605, 1989.

Kerr, Y. H., and R. Magani, Use of the ERS-1 wind-scatterometer data over land surfaces: Arid and semi-arid lands, paper presented at the 2nd ERS-1 Symposium,ESA, Hamburg, Germany, Oct. 11-14, 1993.

Kerr, Y. H., and E. G. Njoku, On the use of passive microwave at 37 GHz in remote sensing of vegetation, *Int. J. Remote Sens.*, *14*, 1931-1943, 1993.

Knipling, E. B., Physical and physiological basis for the re-

flectance of visible and near-infrared radiation from vegetation, Remote Sens. Environ., 1, 155-159, 1970.

Kohonen, T., Self-Organization and Associative Memory, Springer-Verlag, New York, 1984.

Lakshmi, V., E. F. Wood, and B. J. Choudhury, Evaluation of Special Sensor Microwave/ Imager satellite data for regional soil moisture estimation over the Red River Basin, J. Appl. Meteorol., 36, 1309-1328, 1997.

Marticorena, B., G. Bergametti, B. Aumont, Y. Callot, C. N'Doumi, and M. Legrand, Modeling the atmospheric dust cycle. II: Simulation of Saharan dust sources, J. Geophys. Res., 102, 4387-4404, 1997.

Matthews, E., Global vegetation and land use: New high-resolution data bases for climate studies, J. Clim. Appl. Meteorol., 22, 474-486, 1983.

Matzler, C., Seasonal evolution of microwave radiation from an oat field, Remote Sens. Environ., 31, 161-173, 1990.

Moulin, S., L. Kergoat, N. Viovy, and G. Dedieu, Global-scale assessment of vegetation phenology using NOAA/AVHRR satellite, J. Clim., 10, 1154-1170, 1997.

Myneni, R. B., C. J. Tucker, G. Asrar, and C. D. Keeling, Interannual variations in satellite-sensed vegetation index data from 1981 to 1991, J. Geophys. Res., 103, 6145-6160, 1998.

Owe, M., A. A. Van de Griend, R. de Jeu, J. J. de Vries, E. Seyhan, and E. T. Engman, Estimating soil moisture from satellite microwave observations: Past and ongoing projects, and relevance to GCIP, J. Geophys. Res., 104, 19,735-19,742, 1999.

Pinty, B., and G. Szejwach, A new technique for inferring surface albedo from satellite observations, J. Clim. Appl. Meteorol., 24, 741-750, 1985.

Prigent, C., W. B. Rossow, and E. Matthews, Microwave land surface emissivities estimated from SSM/I observations, J. Geophys. Res., 102, 21,867-21,890, 1997.

Prigent, C., W. B. Rossow, and E. Matthews, Global maps of microwave land surface emissivities: Potential for land surface characterization, Radio Sci., 33, 745-751, 1998.

Prigent, C., W. B. Rossow, E. Matthews, and B. Marticorena, Microwave radiometric signatures of different surface types in deserts, J. Geophys. Res., 104, 12,147-12,158, 1999.

Prigent, C., J.-P. Wigneron, W. B. Rossow, and J. R. Pardo-Carrion, Frequency and angular variations of land surface microwave emissivities: Can we estimate SSM/T and AMSU emissivities from SSM/I emissivities, IEEE Trans. Geosci. Remote Sens., 38, 2372-2386, 2000.

Rossow, W. B., and R. A. Schiffer, ISCCP cloud data products, Bull. Am. Meteorol. Soc., 72, 2-20, 1991.

Rossow, W. B., and R. A. Schiffer, Advances in understanding clouds from ISCCP, Bull. Am. Meteorol. Soc., 80, 2261-2287, 1999.

Rossow, W. B., A. W. Walker, D. E. Beuschel, and M. D. Roiter, International Satellite Cloud Climatology Project (ISCCP): Document on new cloud datasets, NASA Goddard Inst. for Space Stud., New York, 1996.

Schaale M., and R. Furrer, Land surface classification by neural networks, Int. J. Remote Sens., 16, 3003-3031, 1995.

Scott, D., P. H. Menalda, and R. W. Brougham, Spectral analysis of radiation transmitted and reflected by different vegetations, N. Z. J. Bot., 6, 427-449, 1968.

Sellers, P. J., C. J. Tucker, G. J. Collatz, S. O. Los, C. O. Justice, D. A. Dazlich, and D. A. Randall, A global 1-deg by 1-deg NDVI data set for climate studies, 2, The generation of global fields of terrestrial biophysical parameters

from the NDVI, Int. J. Remote Sens., 15, 3519-3545, 1994.

Sellers, P. J., S. O. Los, C. J. Tucker, C. O. Justice, D. A. Dazlich, G. J. Collatz, and D. A. Randall, A revised land surface parameterization (SiB2) for atmospheric GCMs, 2, The generation of global fields of terrestrial biophysical parameters from satellite data, J. Clim., 9, 706-737, 1996.

Sinclair, T. R., R. M. Hoffer, and M. M. Schreiber, Reflectance and internal structure of leaves from several crops during a growing season, Agron. J., 63, 864-867, 1971.

Sippel, S. J., S. K. Hamilton, J. M. Melack, and E. M. M. Novo, Passive microwave observations of inundation area and area/stage relation in the Amazon River floodplain, Int. J. Remote Sens., 19, 3055-3074, 1998.

Tanré, D., B. N. Holben, and Y. F. Kaufman, Atmospheric correction algorithm for NOAA-AVHRR products: Theory and application, IEEE Trans. Geosci. Remote Sens., 30, 231-248, 1992.

Tucker, C. J., Red and photographic infrared linear combinations for monitoring vegetation, Remote Sens. Environ., 8, 127-150, 1979.

Tucker, C. J., Comparing SMMR and AVHRR data for drought monitoring, Int. J. Remote Sens., 10, 1663-1672, 1989.

Tucker, C. J., J. R. G. Townshend, and T. E, Goff, African land-cover classification using satellite data, Science, 227, 369-375, 1985.

Ulaby, F. T., R. K. Moore, and A. K. Fung, Microwave Remote Sensing, Active and Passive, vol. 3, Artech House, Norwood, Mass., 1986.

Vinnikov, K. Y., A. Robock, S. Qiu, J. K. Entin, M. Owe, B. J. Choudhury, S. E. Hollinger, and E. G. Njoku, Satellite remote sensing of soil moisture in Illinois, United States, J. Geophys. Res., 104, 4145-4168, 1999.

Wagner, W., G. Lemoine, and M. Borgeaud, A study of vegetation cover effects on ERS scatterometer data, IEEE Trans. Geosci. Remote Sens., 37, 938-947, 1999a.

Wagner, W., J. Noll, M. Borgeaud, and H. Rott, Monitoring soil moisture over the Canadian prairies with the ERS scatterometer, IEEE Trans. Geosci. Remote Sens., 37, 206-216, 1999b.

Wigneron, J.-P., J.-C. Calvet, Y. Kerr, A. Chanzy, and A. Lopes, Microwave emission of vegetation: Sensitivity to leaf characteristics, IEEE Trans. Geosci. Remote Sens., 31, 716-726, 1993.

Wigneron, J.-P., D. Guyon, J.-C. Calvet, G. Courrier, and N. Bruguier, Monitoring coniferous forest characteristics using a multifrequency (5-90 GHz) microwave radiometer, Remote Sens. Environ., 60, 299-310, 1997.

Wismann, V., K. Boehnke, and C. Schmullius, Radar signatures of land surfaces measured by the ERS-1 scatterometer, paper presented at the 2nd ERS-1 Symposium, ESA, Hamburg, Germany, Oct. 11-14, 1993.

C. Prigent, Département de Radioastronomie Millimétrique, Observatoire de Paris, 61, avenue de l'Observatoire, 75014 Paris, France. (catherine.prigent@obspm.fr)

F. Aires, E. Matthews, and W. B. Rossow, NASA Goddard Institute for Space Studies, 2880 Broadway, New York, NY 10025. (faires@giss.nasa.gov; ematthews@giss.nasa.gov; wrossow@giss.nasa.gov)